Optimized analytic reconstruction for SPECT

Jean-Pol Guillement, Roman Novikov

Optimized analytic reconstruction for SPECT

J.-P. Guillement[1], **R.G. Novikov**[2]

[1] CNRS, Laboratoire de Mathématiques Jean Leray (UMR 6629), Université de Nantes, BP 92208, F-44322, Nantes cedex 03, France
E-mail: guillement@math.univ-nantes.fr

[2] CNRS (UMR 7641), Centre de Mathématiques Appliquées, Ecole Polytechnique, 91128 Palaiseau, France
E-mail: novikov@cmap.polytechnique.fr

Abstract

We develop optimized analytic reconstruction for the single-photon emission computed tomography (SPECT). This reconstruction is based on : (1) Novikov's exact and Chang's approximate inversion formulas for the attenuated ray transform, (2) filtering techniques, and (3) Morozov type discrepancy principle. Our numerical examples include comparisons with the standard least square and expectation maximization iterative SPECT reconstructions.

1. Introduction

In the single-photon emission computed tomography (SPECT) one considers a body containing radioactive isotopes emitting photons. The emission data p in SPECT consist in the radiation measured outside the body by a family of detectors during some fixed time. The basic problem of SPECT consists in finding the distribution f of these isotopes in the body from the emission data p and some a priori information concerning the body. Usually this a priori information consists in the photon attenuation coefficient a in the points of body, where this coefficient is found in advance by the methods of the transmission computed tomography.

In addition, it is assumed that:

$$\begin{aligned} &f(x) \geq 0, \quad a(x) \geq 0, \quad x \in \mathbb{R}^d, \\ &supp\, a \subseteq D, \quad supp\, f \subseteq D, \end{aligned} \tag{1.1}$$

where f and a are the aforementioned density of radioactive isotopes and photon attenuation coefficient, D is some known compact domain containing the body; the aforementioned emission data p are defined on the detector set Γ, where Γ is identified with some discrete subset of the set T of all oriented straight lines in $\mathbb{R}^d$; $p(\gamma)$ is the number of photons coming from (the domain containing) the body along oriented straight line γ to the detector associated with γ, where $\gamma \in \Gamma \subset T$.

In some approximation

$$\begin{aligned} &p(\gamma) \text{ is a realization of a Poisson variate } \mathbf{p}(\gamma) \\ &\text{with the mean } M\mathbf{p}(\gamma) = g(\gamma) = CP_a f(\gamma) \text{ for any } \gamma \in \Gamma \\ &\text{and all } \mathbf{p}(\gamma), \quad \gamma \in \Gamma, \quad \text{are independent,} \end{aligned} \tag{1.2}$$

where

$$P_a f(\gamma) = \int_\gamma \exp\left[-\mathcal{D}a(x,\hat{\gamma})\right] f(x) dx, \tag{1.3}$$

where $\hat{\gamma}$ is the direction of γ, dx is standard Euclidean measure on γ,

$$\mathcal{D}a(x,\theta) = \int_0^{+\infty} a(x+t\theta)dt, \quad x \in \mathbb{R}^d, \quad \theta \in \mathbb{S}^{d-1}, \tag{1.4}$$

$C = C_1 t$, where t is the detection time, C_1 is independent of t.

The transform $P_a f$ of (1.2), (1.3) is the attenuated ray transform of f; the transform $\mathcal{D}a$ of (1.3), (1.4) is the divergent beam transform of a.

Although the SPECT problem $p, a \longrightarrow Cf$ arises for a body contained in $\mathbb{R}^d$, $d = 3$, this problem can be restricted to each fixed 2D plane Ξ intersecting the body and identified with $\mathbb{R}^2$.

We recall that $T \approx \mathbb{R} \times \mathbb{S}^1$, where T is the set of all oriented straight lines in $\mathbb{R}^2$. If $\gamma = (s,\theta) \in \mathbb{R} \times \mathbb{S}^1$, then $\gamma = \{x \in \mathbb{R}^2 : \ x = t\theta + s\theta^\perp, \ t \in \mathbb{R}\}$ (modulo orientation) and θ gives the orientation of γ, where $\theta^\perp = (-\theta_2, \theta_1)$ for $\theta = (\theta_1, \theta_2) \in \mathbb{S}^1$.

After the restriction to 2D plane we assume that: (1.1) is fulfilled for $D = \mathcal{B}_R = \{x \in \mathbb{R}^2 : \ |x| \le R\}$, where R is radius of image support; Γ is a uniform $n \times n$ sampling of

$$T_R = \{\gamma \in T : \ \gamma \cap \mathcal{B}_R \neq 0\} = \{(s,\theta) \in \mathbb{R} \times \mathbb{S}^1 : \ |s| \le R\}. \tag{1.5}$$

In addition, the standard value for n is 128.

In the present article we consider the following problem.

Problem 1. Find (as well as possible) Cf from p and a, where Cf, a and p are the functions of (1.2) considered in the framework of the 2D restriction as described above.

More precisely, we continue studies on numerical realizations of explicit analytic reconstruction formulas for Problem 1. In particular, the main result of the present article consists in some optimized analytic reconstruction (for Problem 1) based on Novikov's exact and Chang's approximate formulas for finding f on $\mathbb{R}^2$ from $P_a f$ on T and a on $\mathbb{R}^2$ and on Morozov type discrepancy principle, see Sections 2, 3, 4. Related numerical examples are given in Section 5 containing also comparative studies with some well-known iterative methods. One can see that our optimized analytic reconstruction is rather efficient as regards smallness of its reconstruction error in L^2 norm.

2. Novikov formula

We consider the following exact inversion formula

$$Cf = \mathcal{N}_a g, \tag{2.1}$$

where $g = CP_a f$ is defined as in (1.3) for $d = 2$ and $\gamma = (s,\theta) \in \mathbb{R} \times \mathbb{S}^1$,

$$\mathcal{N}_a q(x) = \frac{1}{4\pi} \int_{\mathbb{S}^1} \theta^\perp \nabla_x K(x,\theta) d\theta, \tag{2.2a}$$

$$K(x,\theta) = \exp\left[-\mathcal{D}a(x,-\theta)\right] \tilde{q}_\theta(x\theta^\perp), \tag{2.2b}$$

$$\tilde{q}_\theta(s) = \exp\big(A_\theta(s)\big)\cos\big(B_\theta(s)\big)\, H(\exp\big(A_\theta\big)\cos\big(B_\theta\big)\, q_\theta\big)(s) + \exp\big(A_\theta(s)\big)\sin\big(B_\theta(s)\big)\, H(\exp\big(A_\theta\big)\sin\big(B_\theta\big)\, q_\theta\big)(s), \tag{2.2c}$$

$$A_\theta(s) = \frac{1}{2} P a(s,\theta), \quad B_\theta(s) = H\, A_\theta(s), \quad q_\theta(s) = q(s,\theta), \tag{2.2d}$$

where q is a test function, $\mathcal{D}a$ is defined by (1.4), $P = P_0$ is the classical two-dimensional ray transformation (i.e. P_0 is defined by (1.3) with $a \equiv 0$), H is the Hilbert transformation defined by the formula

$$H\, u(s) = \frac{1}{\pi}\, p.v. \int\limits_{\mathbb{R}} \frac{u(t)}{s-t} dt, \tag{2.3}$$

where u is a test function, $x = (x_1, x_2) \in \mathbb{R}^2$, $\theta = (\theta_1, \theta_2) \in \mathbb{S}^1$, $\theta^\perp = (-\theta_2, \theta_1)$, $s \in \mathbb{R}$, $d\theta$ is arc-length measure on the circle $\mathbb{S}^1$.

In a slightly different form (using complex notations) formula (2.1) was obtained in [Nov1]. Some new proofs of this formula were given in [Na] and [BS]. Formula (2.1) was successfully implemented numerically in [Ku2] and [Na] via a direct generalization of the (classical) filtered back-projection (FBP) algorithm. However, this generalized FBP algorithm turned out to be considerably less stable, in general, than its classical analogue. Some possibilities for improving the stability of SPECT imaging based on (2.1), (2.2) with respect to the Poisson noise in the emission data g were proposed, in particular, in [Ku2] (preprint version), [GJKNT], [GN1] and [GN2]. Some fast numerical implementation of formula (2.1) was proposed in [BM].

In the present article we suggest new stabilization of the generalized FBP algorithm implementing formula (2.1). This new stabilization involves Morozov's discrepancy principle and Chang's formula, see Sections 3 and 4.

3. Chang formula

We consider the following approximate inversion formula

$$Cf \simeq \mathcal{C}h_a g, \tag{3.1}$$

where $g = CP_a f$ is defined as in (1.3) for $d = 2$ and $\gamma = (s, \theta) \in \mathbb{R} \times \mathbb{S}^1$,

$$\mathcal{C}h_a q(x) = \frac{1}{4\pi w_0(x)} \int\limits_{\mathbb{S}^1} \theta^\perp \nabla_x H q_\theta(x\theta^\perp) d\theta, \tag{3.2a}$$

$$w_0(x) = \frac{1}{2\pi} \int\limits_{\mathbb{S}^1} \exp[-\mathcal{D}a(x,\theta)] d\theta, \tag{3.2b}$$

$$q_\theta(s) = q(s,\theta), \tag{3.2c}$$

where q is a test function, H is defined by (2.3), $\mathcal{D}a$ is defined by (1.4), $x \in \mathbb{R}^2$, $\theta = (\theta_1, \theta_2) \in \mathbb{S}^1$, $\theta^\perp = (-\theta_2, \theta_1)$, $s \in \mathbb{R}$, $d\theta$ is arc-length measure on $\mathbb{S}^1$.

Formula (3.1) is known as Chang's approximate inversion formula for the transformation P_a, see [Ch], [Ku1], [Nov2]. This formula is approximate for the continuous case but

its result is sufficiently stable for reconstruction from discrete and noisy data p of (1.2) on the basis of classical FBP algorithm. It is known that this formula is efficient as the first approximation in SPECT reconstructions, see [Ch], [Ku1], [Nov2].

4. Optimization

The exact formula (2.1) is sufficiently stable on sufficiently low frequency part of p and a but is rather unstable on other part of these data, see [Ku2], [GJKNT]. Therefore, some reasonable low frequency approximation to Cf can be found as

$$Cf \approx Cf_\alpha = \mathcal{N}_{a_\alpha}(\mathcal{W}p)_\alpha \quad \text{or} \tag{4.1a}$$

$$Cf \approx Cf_\alpha = (\mathcal{N}_a(\mathcal{W}p)_\alpha)_\alpha, \tag{4.1b}$$

where $\mathcal{N}_a$ denotes the generalized FBP algorithm implementing (2.2), α is optimization parameter, $\mathcal{W}$ is some moderate filter (for example, space-variant Wiener type filter of [GN2]), a_α, $(\mathcal{W}p)_\alpha$, $(\mathcal{N}_a(\mathcal{W}p)_\alpha)_\alpha$ denote the low-frequency parts of a, $\mathcal{W}p$, $\mathcal{N}_a(\mathcal{W}p)_\alpha$, respectively, obtained via some standard 2D space-invariant low-frequency filtering dependent on α. In addition, according to the Morozov principle we choose α as a parameter minimizing the discrepancy

$$d_\alpha = \|P_a Cf_\alpha - \mathcal{W}p\|_{L^2(\Gamma)}. \tag{4.2}$$

Numerical examples illustrating the reconstruction (4.1) with α found via the Morozov discrepancy principle are given in Section 5, see figure 3 and formula (5.6). As far as we know, these very natural numerical studies were not yet given in the literature.

In addition, the approximate formula (3.1) is sufficiently stable even on reasonably high frequency part of p and a. Therefore, the optimized approximate reconstruction (4.1) can be considerably improved as

$$Cf \approx Cf_\alpha = \mathcal{N}_{a_\alpha}(\mathcal{W}p)_\alpha + \mathcal{C}h_a(\mathcal{W}p - (\mathcal{W}p)_\alpha) \quad \text{or} \tag{4.3a}$$

$$Cf \approx Cf_\alpha = (\mathcal{N}_a(\mathcal{W}p)_\alpha)_\alpha + \mathcal{C}h_a(\mathcal{W}p - ((\mathcal{W}p)_\alpha)_\alpha), \tag{4.3b}$$

where we use notations similar to notations of (2.1), (3.1), (4.1) and where we choose α as a parameter minimizing the discrepancy (4.2) with Cf_α of (4.3). Numerical examples illustrating the reconstruction (4.3) with α found via the aforementioned Morozov-type discrepancy principle are given in Section 5, see figure 4 and formula (5.7).

Note also that some optimized analytic reconstruction based on (2.1), (3.1) can be constructed as

$$Cf \approx Cf_\beta = (1-\beta)Cf^1 + \beta Cf^2, \tag{4.4}$$

where $Cf^1 = Cf_\alpha$ is based on (4.1), $Cf^2 = \mathcal{C}h_a\mathcal{W}p$ and β is a parameter minimizing d_β of (4.2) with Cf_β of (4.4). This reconstruction Cf_β is numerically simpler than the aforementioned reconstruction Cf_α of (4.3). However, the reconstruction result for Cf_α of (4.3) is better than for Cf_β of (4.4), see formulas (5.7),(5.9).

5. Numerical examples

5.1. Preliminary remarks

All 2D images of this article are considered on $n \times n$ grids, where $n = 128$.

We assume that X is uniform $n \times n$ sampling of the domain

$$\mathcal{D}_R = \{x = (x_1, x_2) \in \mathbb{R}^2 : \ \max(|x_1|, |x_2|) \leq R\}$$

and Γ is uniform $n \times n$ sampling of T_R defined by (1.5), where R is radius of image support. We use also the following notations

$$\zeta(q_2, q_1, \Gamma') = \frac{\|q_2 - q_1\|_{L^2(\Gamma')}}{\|q_1\|_{L^2(\Gamma')}}, \tag{5.1}$$

where q_1, q_2 are test functions on $\Gamma' \subseteq \Gamma$ and

$$\eta(u_2, u_1, X') = \frac{\|u_2 - u_1\|_{L^2(X')}}{\|u_1\|_{L^2(X')}}, \tag{5.2}$$

where u_1, u_2 are test functions on $X' \subseteq X$.

Given f and a on X, we assume that $P_a f$ is defined on Γ and is numerical realization of (1.3) as in [Ku2]. Given a on X and q on Γ, we assume that $\mathcal{N}_a q$ and $\mathcal{C}h_a q$ are defined on X and denote the numerical realizations of (2.2) and (3.2) on the basis of generalized and classical FBP algorithms, respectively, see [Ku2].

We assume that $\hat{q} = Fg$ denotes the discrete Fourier transform of q.

All 2D images of the present article, except the spectrum of projections, are drawn using a linear greyscale, in such a way that the dark grey color represents zero (or negative values, if any) and white corresponds to the maximum value of the imaged function. For the spectrum of projections, a non-linear greyscale was used, because of too great values of the spectrum for small frequencies.

5.2. Elliptical chest phantom

We consider a version of the elliptical chest phantom (used for numerical simulations of cardiac SPECT imaging; see [HL], [Br], [GN1]). This version is, actually, the same that in [GN1], [GN2] and its description consists in the following:

(1) The major axis of the ellipse representing the body is 30 cm.

(2) The attenuation map is shown in figure 1(a); the attenuation coefficient a is 0.04 cm^{-1} in the lung regions (modeled as two interior ellipses), 0.15 cm^{-1} elsewhere within the body ellipse, and zero outside the body.

(3) The emitter activity f is shown in figure 1(b); f is in the ratio 8:0:1:0 in myocardium (represented as a ring), lungs, elsewhere within the body, and outside the body.

(4) The attenuated ray transform $g = CP_a f$ and noisy emission data p of (1.2) are shown in figures 1(c), 2(a). In addition, the constant C was specified by the equation

$$\|g\|_{L^1(\Gamma)} / \|g\|^2_{L^2(\Gamma)} = (0.30)^2 \tag{5.3}$$

in order to have that the noise level $\zeta(p, g, \Gamma) \approx 0.30$ (where ζ is defined by (5.1)). Actually, we have that

$$\zeta(p, g, \Gamma) = 0.298, \quad \sum_{\gamma \in \Gamma} p(\gamma) = 125450 \tag{5.4}$$

for p shown in figure 2(a), where ζ is defined by (5.1).

Figures 1(d) and 2(b) show the spectrums $|\hat{g}|$ and $|\hat{p}|$.

5.3. Reconstruction results

Figures 2(c), 2(d) show the filtering result $\mathcal{W}p$ and its spectrum $|\widehat{\mathcal{W}p}|$ (for p shown in figure 2 (a)) for $\mathcal{W} = \mathcal{A}^{sym}_{8,8}$, where $\mathcal{A}^{sym}_{l_1,l_2}$ is the approximately optimal space-variant Wiener-type filter of Section 5.3 of [GN2]. In addition,

$$\zeta(\mathcal{W}p, g, \Gamma) = 0.110 \tag{5.5}$$

which is about three times smaller than ζ of (5.4).

Figures 3, 4 show the reconstructions Cf_α of (4.1a), (4.3a) and their central horizontal profiles, where $\mathcal{W} = \mathcal{A}^{sym}_{8,8}$ and α is found, for each of these reconstructions, as a parameter minimizing d_α of (4.2). In addition,

$$\eta(Cf_\alpha, Cf, X) = 0.445 \text{ for } \mathrm{Cf}_\alpha \text{ of (4.1a)}, \tag{5.6}$$

$$\eta(Cf_\alpha, Cf, X) = 0.367 \text{ for } \mathrm{Cf}_\alpha \text{ of (4.3a)}, \tag{5.7}$$

where Cf is, actually, shown in figure 1(b), η is defined by (5.2).

We have also that:

$$\eta(Cf^2, Cf, X) = 0.393 \tag{5.8}$$

for $Cf^2 = \mathcal{C}h_a\mathcal{W}p$ of (4.4), where $\mathcal{W} = \mathcal{A}^{sym}_{8,8}$;

$$\eta(Cf_\beta, Cf, X) = 0.391 \tag{5.9}$$

for Cf_β of (4.4), where $\mathcal{W} = \mathcal{A}^{sym}_{8,8}$ and β is found as a parameter minimizing d_β of (4.2).

An efficiency of (3.1), confirmed by (5.8), is explained in particular in [Nov2].

Figures 5(a)-(d) show standard steepest descent least square (SDLS) and expectation maximization (EM) reconstructions Cf_{rec} and their central horizontal profiles, obtained via 60 iterations of each of these methods from a and p shown in figures 1(a), 2(a). In addition,

$$\eta(Cf_{rec}, Cf, X) = 0.436 \text{ for the SDLS case}, \tag{5.10}$$

$$\eta(Cf_{rec}, Cf, X) = 0.421 \text{ for the EM case}, \tag{5.11}$$

where η, Cf, X are the same that in (5.6)-(5.9). For description of EM method in emission tomography, see [HL], [SV] and references therein.

One can see that in our numerical examples Cf_α of (4.3a) is the best as regards smallness of the reconstruction error in L^2 norm, whereas Cf_{rec} obtained via 60 EM iterations is the best as regards the resolution. Possible optimizations of EM and SDLS reconstructions with respect to the iteration number will be not discussed in the present article.

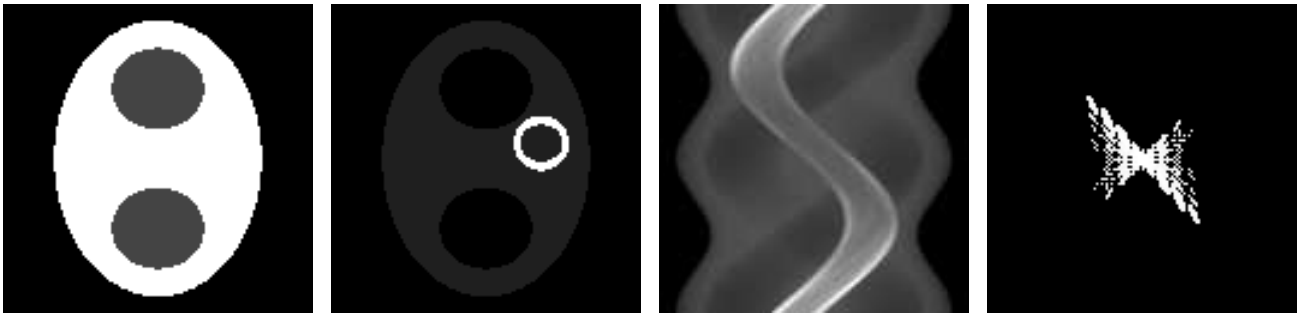

(a) (b) (c) (d)

Figure 1. Attenuation map a (a), emitter activity f (b), noiseless emission data $g = CP_a f$ (c), spectrum $|\hat{g}|$ (d). (See Section 1 and Subsection 5.2.)

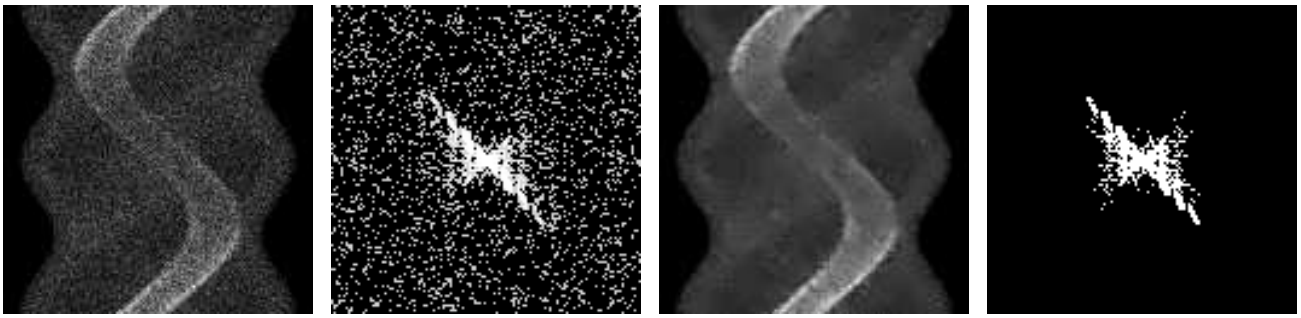

(a) (b) (c) (d)

Figure 2. Noisy emission data p (a), spectrum $|\hat{p}|$ (b), filtering result $\mathcal{W}p$ (c), spectrum $|\widehat{\mathcal{W}p}|$ (d), for $\mathcal{W} = \mathcal{A}_{8,8}^{sym}$. (See Sections 1, 4 and Subsections 5.2, 5.3.)

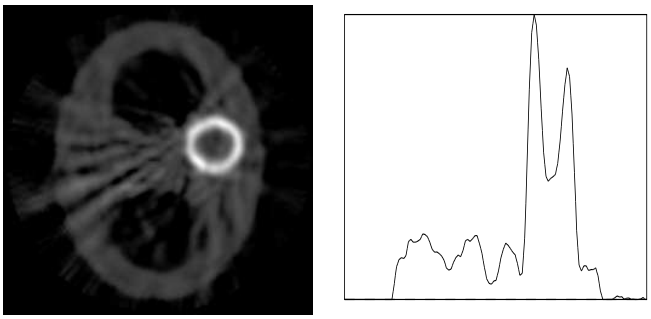

(a) (b)

Figure 3. Reconstruction Cf_α of (4.1a) (a) with its central horizontal profile (b). (See Section 4 and Subsection 5.3.)

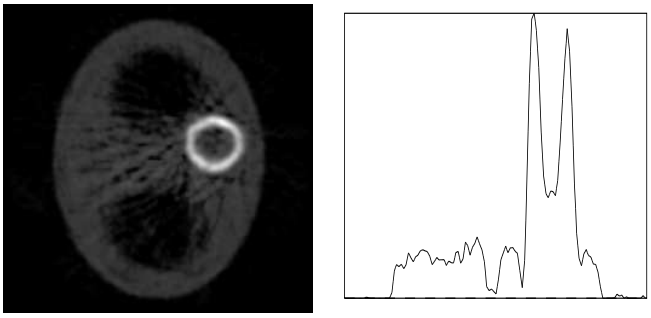

(a) (b)

Figure 4. Reconstruction Cf_α of (4.3a) (a) with its central horizontal profile (b). (See Section 4 and Subsection 5.3.)

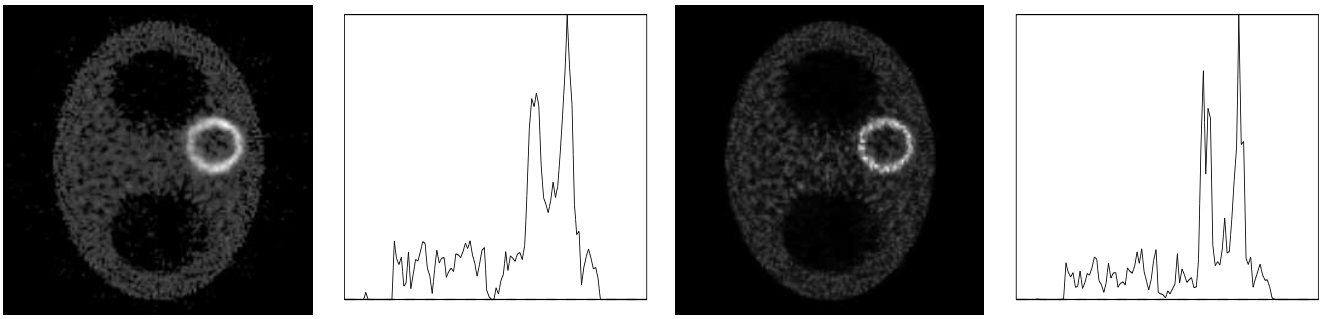

(a) (b) (c) (d)

Figure 5. Reconstruction Cf_{rec} by 60 SDLS iterations(a), by 60 EM iterations (c), and their central horizontal profiles (b), (d). (See Section 1 and Subsection 5.3.)

6. Conclusions

In this work we developed optimized analytic reconstructions based on : (1) Chang's approximate and Novikov's exact inversion formulas for the attenuated ray transform, see formulas (2.1), (3.1); (2) filtering techniques including Wiener-type filters of [GN2]; (3) Morozov type discrepancy principle. The formulas of these optimized analytic reconstructions are given in Section 4 and related numerical examples are given in Section 5.

One can see that, for example, our optimized analytic reconstruction Cf_α of (4.3) is quite competitive with classical iterative (SDLS and EM) methods as regards the reconstruction error in L^2 norm, see formulas (5.7), (5.10), (5.11). However, the classical EM method works better as regards the resolution, see figures 4 and 5(c), 5(d).

Thus, improving resolution properties of analytic reconstructions in SPECT is an open direction for researches.

References

[BM] Bal G and Moireau P 2004 Fast numerical inversion of the attenuated Radon transform with full and partial measurements *Inverse Problems* **20** 1137-1164

[BS] Boman J and Strömberg J O 2004 Novikov's inversion formula for the attenuated Radon transform - A new approach *Journal of Geometric Analysis* **14** 185-198

[Br] Bronnikov A.V. 2000 Reconstruction of attenuation map using discrete consistency conditions *IEEE Trans. Med. Imaging* **19** 451-462

[Ch] Chang L.T 1978 A method for attenuation correction in radionuclide computed tomography *IEEE Trans. Nucl. Sci.* **25** 638-643

[GJKNT] Guillement J-P, Jauberteau F, Kunyansky L, Novikov R and Trebossen R 2002 On single-photon emission computed tomography imaging based on an exact formula for the nonuniform attenuation correction *Inverse Problems* **18** L11-L19

[GN1] Guillement J-P and Novikov R G 2004 A noise property analysis of single-photon emission computed tomography data *Inverse Problems* **20** 175-198

[GN2] Guillement J-P and Novikov R G 2008 On Wiener type filters in SPECT *Inverse Problems* **24** 025001 (26 pp)

[HL] Hudson H M and Larkin R S 1994 Accelerated image reconstruction using ordered subsets of projection data *IEEE Trans. Med. Imaging* **13** 601-609

[Ku1] Kunyansky L A 1992 Generalized and attenuated Radon transforms: restorative approach to the numerical inversion *Inverse Problems* **8** 809-819

[Ku2] Kunyansky L A 2001 A new SPECT reconstruction algorithm based on the Novikov's explicit inversion formula *Inverse Problems* **17** 293-306 (E-print, m*p*_arc/00-342)

[Na] Natterer F 2001 Inversion of the attenuated Radon transform *Inverse Problems* **17** 113-119

[Nov1] Novikov R G 2002 An inversion formula for the attenuated x-ray transformation *Ark. Mat.* **40** 145-167 *Inverse Problems* **18** 677-700

[Nov2] Novikov R G 2011 Weighted Radon transforms for which Chang's approximate inversion formula is exact. Uspekhi Mat. Nauk **66** (2) 237-238

[SV] Shepp L A and Vardi Y 1982 Maximum likelihood reconstruction for emission tomography *IEEE Trans. Med. Imaging* **2** 113-122